Molecular Biophysics:

Color-tuned Channelrhodopsins for Multiwavelength Optogenetics

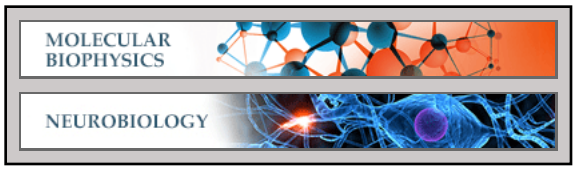

Matthias Prigge, Franziska Schneider, Satoshi P. Tsunoda, Carrie Shilyansky, Jonas Wietek, Karl Deisseroth and Peter Hegemann

J. Biol. Chem. 2012, 287:31804-31812.
doi: 10.1074/jbc.M112.391185 originally published online July 27, 2012

THE JOURNAL OF BIOLOGICAL CHEMISTRY VOL. 287, NO. 38, pp. 31804–31812, September 14, 2012

Color-tuned Channelrhodopsins for Multiwavelength Optogenetics[S]

Received for publication, June 13, 2012, and in revised form, July 23, 2012 Published, JBC Papers in Press, July 27, 2012, DOI 10.1074/jbc.M112.391185

Matthias Prigge[‡1], Franziska Schneider[‡1], Satoshi P. Tsunoda[‡], Carrie Shilyansky[§], Jonas Wietek[‡], Karl Deisseroth[§2], and Peter Hegemann[‡3]

From the [‡]Institute of Biology, Experimental Biophysics, Humboldt-Universität zu Berlin, 10115 Berlin, Germany and the [§]Departments of Bioengineering and Psychiatry, Howard Hughes Medical Institute, Computer Numerical Control Program, Stanford University, Stanford, California 94305

Background: Dual-color activation of two cell types with channelrhodopsins is a major challenge because all available well expressing variants absorb blue light.
Results: We engineered channelrhodopsin hybrids with color-shifted spectra, as well as altered kinetics and selectivity.
Conclusion: The results provide deeper insight into channelrhodopsin function.
Significance: The combination of novel and established channelrhodopsins can activate distinct cell populations by dual-color excitation.

Channelrhodopsin-2 is a light-gated ion channel and a major tool of optogenetics. It is used to control neuronal activity via blue light. Here we describe the construction of color-tuned high efficiency channelrhodopsins (ChRs), based on chimeras of *Chlamydomonas* channelrhodopsin-1 and *Volvox* channelrhodopsin-1. These variants show superb expression and plasma membrane integration, resulting in 3-fold larger photocurrents in HEK cells compared with channelrhodopsin-2. Further molecular engineering gave rise to chimeric variants with absorption maxima ranging from 526 to 545 nm, dovetailing well with maxima of channelrhodopsin-2 derivatives ranging from 461 to 492 nm. Additional kinetic fine-tuning led to derivatives in which the lifetimes of the open state range from 19 ms to 5 s. Finally, combining green- with blue-absorbing variants allowed independent activation of two distinct neural cell populations at 560 and 405 nm. This novel panel of channelrhodopsin variants may serve as an important toolkit element for dual-color cell stimulation in neural circuits.

Channelrhodopsins (ChRs)[4] are photoreceptors that control photomovement in green algae. ChRs are small monomeric ion channels (1) that can be functionally expressed in defined cell populations in living animals ranging from nematodes, fruit flies, mice, zebrafish, to primates (2–5). ChR has also generated hope for clinical applications such as for recovery of rudimentary vision in blind patients (retinal prosthesis), deep brain stimulation for treatment of Parkinson disease, treatment of heart failure by light-induced pacing, peripheral nerve stimulation, and modulation of fear learning (6–10).

Upon light stimulation, ChR conductance comprises an initial current, I_0, which decays to a steady-state current, I_S Relaxation from I_0 to I_S is commonly called inactivation of the conductance, although these kinetics are in fact the result of an early and a late conducting state (O1 and O2) within the ChR photocycle (11). Correspondingly, the off-kinetics comprise several exponentials in principle, but are frequently well described at physiological conditions by one exponential (2). Despite the wide application of ChR, the use of channelrhodopsin-2 (C2) bears several limitations that often prevent sufficient depolarization in optogenetic studies. These are, for example, low expression levels, small unitary conductance, inappropriate kinetics, partial inactivation, and inappropriate ion selectivity. Moreover, simultaneous application of the actuator C2 and fluorescent sensors or separate activation of two cell types with different ChRs is still a challenge.

In several approaches ChRs have been tailored for modulated absorption, kinetics, and membrane targeting. Because of the fact that the retinal-binding pocket is conserved in all microbial rhodopsins, we first modified amino acids that are in close contact with the retinal. Replacement of the active site residue Glu-123 by Thr and Ala (ChETA variants) caused faster channel closing, eliminated the voltage sensitivity of the temporal kinetics, and induced a 20-nm bathochromic shift (12). In contrast, substitution of Cys-128 by Ser, or of Asp-156 by Ala or combination of both led to an extreme extension of the open state lifetime with τ_{off} values up to 30 min and allowed on/off switching with dual wavelength light protocols (13–15). Mutation of Glu-90, Glu-123, Leu-132, or His-134 does not change photocycle kinetics but alters ion selectivity in favor of H^+, Na^+, or Ca^{2+}, or reduces inactivation after light step-up or multiple light flashes, respectively (16, 17). A helix swapping approach combining structural elements from C1 and C2 led to improved ChRs with larger currents, absorption maxima at approximately 500 nm, and reduced inactivation (18). Moreover, screening of a genomic database led to the identification of

[S] This article contains supplemental Figs. 1–3 and Tables 1–3.
[1] Both authors contributed equally to this work.
[2] Supported, in whole or in part, by the National Institutes of Health. Also supported by the Howard Hughes Medical Institute, the Gatsby Foundation, and the DARPA REPAIR program (reorganization and plasticity to accelerate injury recovery).
[3] Supported by the German Research Foundation and Deutsche Forschungsgemeinschaft Grants HE3824/9-3 and 9-4. To whom correspondence should be addressed. Tel.: 0049-30-2093-8681; E-mail: hegemape@rz.hu-berlin.de.
[4] The abbreviations used are: ChR, channelrhodopsin; C1 and C2, channelrhodopsin-1 and -2, respectively; V1 and V2, Volvox channelrhodopsin-1 and 2.

Volvox C1 in the following named V1 with an absorption maximum at 535 nm (19, 20). When expressed in pyramidal neurons, V1 could evoke action potentials with 590-nm light, but widespread use was hampered by low expression in most neuronal cell types. Up until now, experiments in which distinct neuronal populations were separately controlled by dual-color activation are rare but have been demonstrated for the depolarizing C2 in combination with the hyperpolarizing red-absorbing chloride pump halorhodopsin from *Natronomonas pharaonis* (21). Dual-color depolarization experiments require multiple sets of ChR variants with spectrally well separated absorption, large photocurrents, and perhaps even different operational light sensitivities. Operational light sensitivity is defined by the light power necessary to evoke action potentials in neurons and depends on ChR expression, kinetics, ion selectivity, and conductance, as well as on endogenous cellular characteristics. Operational light sensitivity also subsumes the intrinsic light sensitivity of the actuator in charge, which, however, is quite invariant for all microbial rhodopsins. Advanced optogenetics will not only depend on actuator probes, but also on the simultaneous use of reporter proteins as genetically encoded fluorescent calcium indicators or voltage sensors. To meet this challenge, we implemented a systematic molecular engineering approach, integrating helix swapping as global rearrangement of structural elements with subsequent mutagenesis resulting in local conformational changes or alteration of the hydrogen bond network. This allows us to present a broader color palette of ChRs to fill the gap effectively. The best candidates were tested in hippocampal neurons to validate usability in different cell types. The recently described three-dimensional structure of a distinct C1C2 chimera allows to interpret our results on a molecular level (22).

EXPERIMENTAL PROCEDURES

Molecular Biology—Chimeric ChR variants were generated from synthetic human codon-adapted cDNAs of ChR-encoding genes named in the algal database *Chlamydomonas* opsins (*COP*): *COP3*, *COP4* encoding ChR1 (C1) and CHR2 (C2) (GenBank EU714030.1), and the volvoxopsins *VOP3* and *VOP4* encoding VChR1 (V1) and VChR2 (V2). DNA fragments were combined by overlap extension PCR as described elsewhere (18). Resulting PCR fragments were cloned in-frame into pECFP-N1 using XbaI/BamHI. Junction sites of chimeras are summarized in supplemental Table 2. Point mutations were generated with QuikChange (Agilent Technologies, Palo Alto, CA). For oocyte measurements chimera were subcloned into the pGEMHE vector with BamHI/BsiWI. A full-length cRNA was synthesized *in vitro* from NheI-linearized pGEMHE plasmid using T7 RNA polymerase (mMessage mMachine; LifeTechnologies).

HEK Cell Recording—HEK293 cells were cultured as described (24) and seeded onto coverslips at a concentration of 0.175×10^6 cells·ml^{-1} and supplemented with 1 μM all-*trans*-retinal. Transient transfection was performed using FuGENE 6 (Roche Applied Science) 20–28 h before measurements. For selectivity measurements a cell line stably expressing C2-mVenus was used (14). Signals were amplified and digitized using AxoPatch200B or Heka EPC7 and DigiData1440. For recording wavelength dependence a light guide from a Polychrome V unit (TILL Photonics, Planegg, Germany) was mounted at the epi-illumination port of an Olympus IX70 microscope resulting in a final light intensity between 0.05 and 0.23 mW·mm^{-2} for 380–650 nm on the coverslip. Action spectra as shown in Fig. 1*C* were recorded at 50% of the maximum light intensity with a bandwidth of 7 nm. The Polychrome V unit was controlled via the Tillvision software (TILL Photonics) synchronized with the pClamp software. For dual excitation a 75-W xenon lamp (Jena Instruments, Jena, Germany) was coupled into the epi-illumination port using a beam splitter (70%/30%). Illumination with the xenon lamp was controlled via a fast shutter (Uniblitz LS3T2, Rochester, NY) controlled by the pClamp software. To record inactivation spectra of slow mutants as shown in supplemental Fig. 1 the intensity of inactivation light was adjusted to an equal number of photons ($7{\cdot}10^{23}$ s^{-1} m^{-2}) for all wavelengths using a software controlled, motorized neutral density filter wheel (Newport, Irvine, CA). For ion selectivity experiments, as shown in Fig. 3*E*, whole cell patch clamp measurements were performed on a HEK cell line stably expressing C2-mVenus or transiently transfected HEK293 cells. Light activation was achieved using a 75-W xenon arc lamp (Leistungselektronik Jena GmbH, Germany) coupled into the optical path of an Axiovert 35 inverted microscope (Carl Zeiss, Jena, Germany) and regulated by a programmable shutter system. Wavelengths were selected via the following set of filters: BP546 ± 15 nm for C1V1 variants and BP470 ± 20 nm for C2 variants resulting in light intensities of 0.68 mW·mm^{-2} at 546 ± 15 nm and 1.71 at 470 ± 20 nm in the object plane, respectively. The standard external solution contained 140 mM NaCl, 2 mM $CaCl_2$, 2 mM $MgCl_2$, 2 mM KCl with 10 HEPES (pH_o 7.2). The standard internal solution contained 110 mM NaCl, 10 mM EGTA, 2 mM $MgCl_2$, 1 mM $CaCl_2$, 5 mM KCl, and 10 HEPES (pH_i 7.2). Buffer composition for ion selectivity measurements is summarized in supplemental Table 3. All buffers were pH-adjusted with CsOH/*N*-methyl-D-glucamine as nonconducted base or HCl, and the final osmolarity was brought to 320 mosM (extracellular solutions) or 290 mosM (intracellular solutions) with glucose.

Calcium Imaging—For fluorescence excitation a light guide of the Polychrome V unit was mounted at the epi-illumination port. For ChR activation a xenon lamp (Jena Instruments, Jena, Germany) was used. Light wavelength was selected by a bandpass filter centered at either 405, 470, or 560 nm with a half band width of 30 nm. Light was coupled into a 3-mm plastic light guide also mounted into the epi-illumination path of the microscope and combined with the beam from the polychrome unit via a 70% R/30% T beam splitter. Combined fura-2 and C2 excitation light was guided to the objective via a dualband dichroic mirror (FF493/574, AF-Analysetechnik, Tübingen, Germany). This allowed us to excite fura-2 at 380 nm and monitor fluorescence between 493 and 535 nm. Using the same filter, C2 could be excited at 405, 470, and 560 nm with 0.03, 0.8, and 0.17 mW·mm^{-2}. Fura-2 excitation was reduced to 0.005 mW·mm^{-2}. Fura-2 fluorescence was recorded with a CCD Imago camera (TILL Photonics). For measurements of light-induced opening of $Ca_V3.2$ (Fig. 3*C*) recordings were performed at the following ion composition: 140 mM NaCl, 2 mM

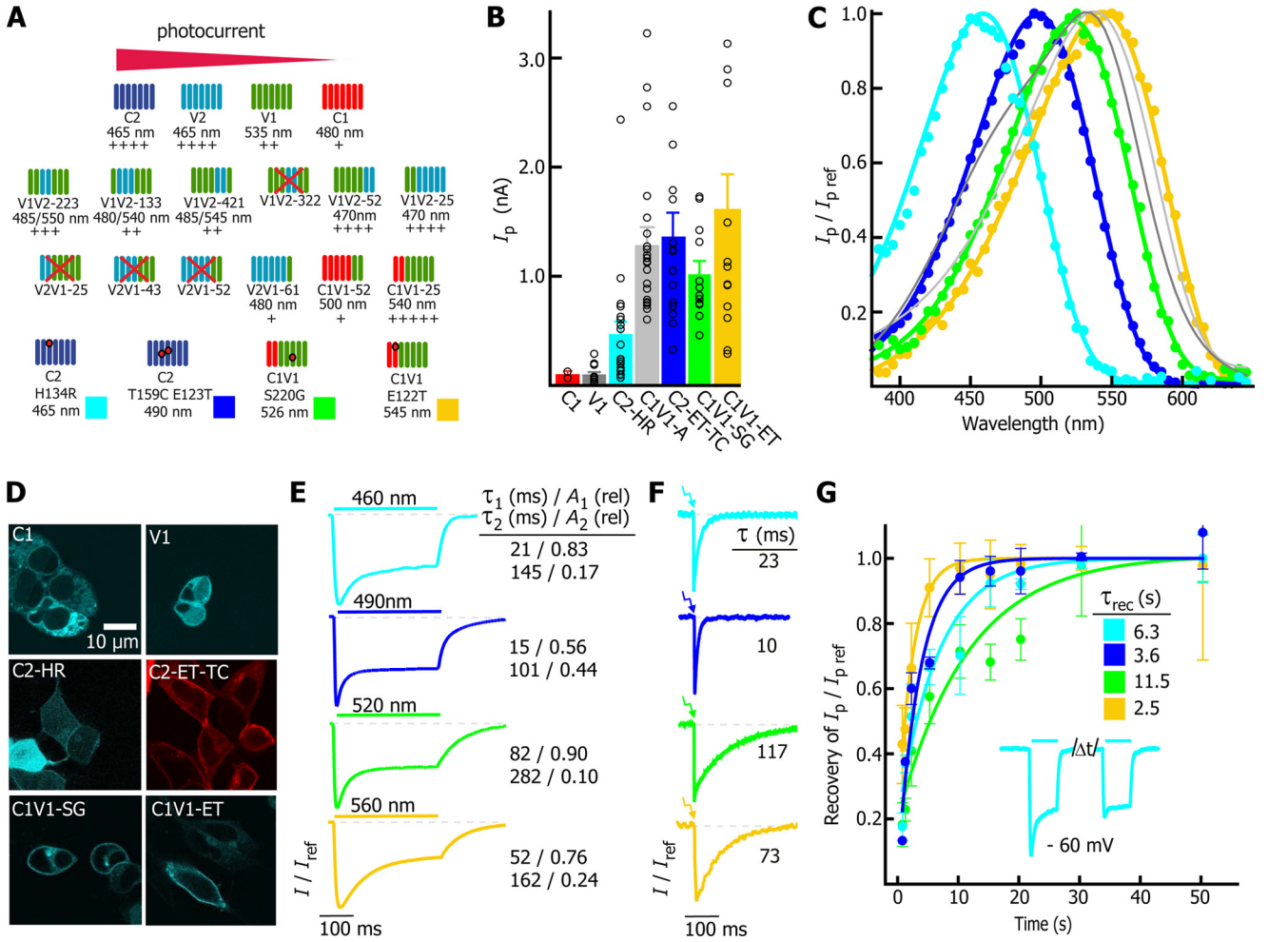

FIGURE 1. **Engineering of ChR chimeras with different spectral properties.** *A*, color-coded ChR chimeras. Peak photocurrent amplitudes are qualitatively indicated by +, and peak absorption wavelengths are given *numerically*. In the cases where two wavelength *numbers* are listed they reflect two distinct maxima recorded at pH_o 5 and 9, that overlap at pH_o 7 and broaden the spectrum. *B*, averaged peak photocurrent amplitudes for all high efficiency color-tuned ChRs and their parental origins in HEK cells. *C*, action spectra of color-tuned ChR variants compared with action spectra of V1 (*dark gray*) exhibiting a *blue shoulder* and C1V1 (*light gray*) (n = 5, 3, 5, 8, 3, and 3 for C2-HR, C2-ET-TC, V1, C1V1-A, C1V1-SG, and C1V1-ET). Amplitudes were linearly corrected to light intensities. *D*, confocal images of HEK cells expressing color variants and their parental ChRs. *E* and *F*, normalized photocurrents upon pulse (in HEK cells) or laser flash stimulation (in *Xenopus* oocytes) for all color mutants. Photocurrents decay biexponentially after activation for 300 ms whereas off-kinetics of dark-adapted ChRs after laser activation can be fitted by a single exponential. Respective τ_{off} values and their relative amplitudes are given numerically. *G*, recovery kinetics of the transient peak in a two-pulse experiment at pH_o 7.2 for color mutants. Between pulses membrane voltage was kept at −60 mV (n = 4, 4, 4, and 3 for C1V1-ET, C2-ET-TC, C2-HR, and C1V1-SG). A typical photocurrent trace is shown as an *inset* (*light blue*).

KCl, 2 mM $MgCl_2$, 2 mM $CaCl_2$, and 10 mM HEPES. pH was adjusted to 7.2 with *N*-methyl-D-glucamine/HCl. Fura-2 fluorescence was recorded at an exposure time of 500 ms at 380 nm and a sampling rate of 0.3 Hz. ChRs were excited for 100 ms with the indicated wavelengths. For experiments testing calcium selectivity of different ChR variants (Fig. 3*G*), cells were measured in the following buffer: 5 mM NaCl, 1 mM KCl, 2 mM $MgCl_2$, 10 mM HEPES, and 70 mM $CaCl_2$. Fura-2 fluorescence was recorded at 380 nm with an exposure time of 500 ms and a sampling rate of 0.3 Hz. ChRs were excited with their corresponding wavelength for 10 s. ΔF over F_0 was calculated as given in Tian *et al.* (25).

Oocyte Photostimulation and Recording—*Xenopus* oocytes (Ecocyte Bioscience, Castrop-Rauxel, Germany) were injected with 50 nl of ChR cRNA (0.5–1 $\mu g \cdot \mu l^{-1}$) and incubated in the dark at 18 °C in Ringer's solution for 3–5 days. Two-electrode voltage clamp measurements were performed on *Xenopus* oocytes using a Turbo Tec-05X (NPI Electronic) and a DigiData 1440A interface. For fast kinetic analysis, cells were stimulated with a tuneable 7-ns laser as described previously (19).

Electrophysiology in Hippocampal and Cortical Neurons—Primary cultured hippocampal neurons were prepared from P0 Sprague-Dawley rat pups (Charles River). CA1 and CA3 were isolated, digested with 0.4 $mg \cdot ml^{-1}$ papain (Worthington), and plated onto glass coverslips precoated with 1:30 Matrigel (BD Biosciences Labware), and grown on coverslips in a 24-well plate at a density of 65,000 cells/well. DNA was expressed in hippocampal pyramidal neurons *in vitro*. DNA maps and clones are available from the Optogenetics. Transfections were carried out 6–10 days after culturing. For each well, a buffered DNA-$CaPO_4$ mix was prepared and incubated at room temperature for 20 min. The mix was added dropwise into each well (from which the growth medium had been removed and replaced with prewarmed minimal essential medium (MEM)), and transfection proceeded for 45–60 min at 37 °C, after which each well was washed, and the original growth medium was

returned. Standard electrophysiology recordings were carried out on day 4–6 after transfection.

Recordings from individual neurons identified by fluorescent protein expression were obtained in Tyrode medium (150 mM NaCl, 4 mM KCl, 2 mM $MgCl_2$, 10 mM D-glucose, 10 mM HEPES, 0.001 mM tetrodotoxin, pH 7.35 with NaOH) using a standard internal solution (130 mM potassium gluconate, 10 mM KCl, 10 mM HEPES, 10 mM EGTA, 2 mM $MgCl_2$, pH 7.3 with KOH) in 3–5-megohm glass pipettes. Rhodopsins were activated by color-filtered light from a xenon lamp source (Sutter Instrument DG-4) that was attenuated by neutral density filters. A minimum of 30-s delay was imposed between stimulus sweeps to minimize confounding effects of inactivation.

Confocal Microscopy—Cells were imaged 1 day after transfection. Pictures were taken on a confocal Olympus LSM IX81 equipped with a 60 × 1.2 Water UplanSApo objective. 440 and 561 nm LEDs were used for excitation. Fluorescence emission was detected using a spectral PMT detector.

Data Analysis—Data were analyzed using Tillvision software or pClamp10.1 and further processed by SigmaPlot and Adobe illustrator. Standard errors are given for all results. Initial currents I_0 were determined by linear extrapolation to $t = 0$. I_P represents peak current; I_S reflects average current after 300 ms of light activation. Action spectra were normalized linearly on the light intensity at each wavelength.

RESULTS

To engineer a highly expressing ChR with large photocurrents and absorption red-shifted relative to ChR2 (C2), we started with VChR1 (V1) because this protein exhibited the most red-shifted absorption spectrum of all known ChRs at the beginning of the project (Fig. 1*C*, *dark gray*). The spectral broadening is based on the simultaneous occurrence of the alkaline and acidic isoforms at neutral, external pH_o (20). Because V1 is only poorly targeted to the membrane in mammalian host cells (Fig. 1*D*), we followed the strategy of Yawo and colleagues by exchanging helices of V1 with homologous helices of related ChRs (18). In a first set of experiments we systematically replaced helices of V1 by helices of the highly expressing *Volvox* VChR2 (*V2*, Fig. 1*A*, *second row*). Exchange of helices H3 and H4, H2 to H4, or H5 and H6 resulted in hybrids with 1.5-fold increased photocurrents in HEK cells and V1-like pH_o-dependent absorption spectra still overlapping at neutral pH_o. Interestingly, chimeras with H6 and H7 of V2 (V1V2–52[5] and V1V2–25) expressed well and exhibited large photocurrents, but the spectra were blue-shifted to 470 nm (Fig. 1*A*). For further improvement, we tested constructs employing N-terminal helices of either V2 or C1 (Fig. 1*A*, *third row*). Chimeras V2V1-25, V2V1-43, and V2V1-52 were nonfunctional in HEK cells. V2V1-61 was functional, but without any improvement over V1. Because several C1C2 chimeras had shown good photocurrents in previous studies we constructed chimeras with N-terminal helices of C1 (18). C1V1-52 integrated exceptionally well into the membrane, but photoconductance was still small and in the range of WT V1. Finally, we restricted the C1 part to the first two helices, which still resulted in a variant with excellent membrane integration (supplemental Fig. 1*A*). This, so called, C1V1-25 variant, was originally prepared as two variants, namely C1V1-25A with the first extracellular loop (ECL1) of C1 and C1V1-25B with ECL1 of V1 (supplemental Fig. 1*A*). For the sake of simplicity, C1V1-25A will be named C1V1 in the following text. Both constructs were again well targeted to the membrane but the B variant elicited larger photocurrents beyond 2000 pA (see Fig. 3*D*, *dark gray*). We have previously reported on aspects of these constructs in the context of neuronal application (15); most of the mutants reported here are based on the original C1V1-25A. For color tuning of C1V1 we replaced Glu-122 for Thr (Glu-83 in C2) in helix H2, a residue that is part of the inner gate and in indirect contact with the chromophore (22). This mutant C1V1-ET exhibited large photocurrents with only moderate inactivation and excellent membrane targeting (Fig. 1*D* and supplemental Table 1). The spectrum showed an additional red shift to $\lambda_{max} = 545$ nm (Fig. 1*C*, *orange*). To fill the spectral gap between the current-improved C2 variant C2-ET-TC (E123T,T159C) with peak absorption near 495 nm (23), and C1V1-ET (E122T) (Fig. 1*C*, *dark blue* and *orange*) we exchanged in C1V1 the polar Ser-220 near the β-ionone ring by an unpolar Gly (see Fig. 2*A* for position). The resulting C1V1-S220G (C1V1-SG) retained its large photocurrent (Fig. 1*B*, *green*), and the spectrum was 13-nm blue-shifted toward 526 nm (Fig. 1*C*).

In Fig. 1, *E* and *F*, representative current traces for light pulses and laser flashes are shown for the well expressing color variants. The C1V1-SG and C1V1-ET off-kinetics in flash experiments ($\tau \approx 117$ and 73 ms) were close to the value for C1V1 ($\tau \approx 77$ ms). But, recovery of the peak current was fast in the case of C1V1-ET ($\tau \approx 2.5$ s) and slow in the case of C1V1-SG ($\tau \approx 11$ s) (Fig. 1*G*, *yellow* and *green*) compared with unmodified C1V1 ($\tau \approx 4$ s). Except for C2-ET-TC, the recovery of the initial current I_0 in C2 and all C1V1 derivatives is slower at more positive voltage (supplemental Fig. 1, *D* and *F*). To change the open-state lifetime of the new color variants, we extended the mutational study with a focus on slow-cycling ChRs (Fig. 2*A*). Replacement of Asp-195 by Ala in C1V1 (D156A in C2) led to a reduction of the current size without any slowdown of the photocycle (τ_{off} ~86 ms), whereas Ser at position Cys-167 (C128S in C2) caused a 40-fold larger τ_{off} (~4 s) (supplemental Table 1). The slowdown of C167S is still 25 times smaller compared with the effect in the corresponding C2 mutation, and it was conceivable that the insensitivity of the photocycle kinetics is caused by the neighboring Cys-198, which is Thr in C2 (Thr-159). We tested this possibility in C2 by introducing T159C on the C2-C128S background in C2, which caused current enlargement with acceleration of the photocycle with an open-state life time of 4 s compared with 106 s in support of our hypothesis (supplemental Fig. 3*B*). To produce color variants with slow kinetics, the color-tuned C1V1-ET (E122T) and C1V1-SG were combined with the C167S mutation (Fig. 2*A*). The double mutants, C1V1-ET-CS and C1V1-CS-SG, showed small photocurrents and off-kinetics between 1.5 and 4.5 s (Fig. 2*B*). The current reduction is most readily explained by a strong overlap of the red-shifted dark state with the conducting state (Pro-520 in C2), which causes immediate photochemical back-reaction in continuous light at all wavelengths between 520 and

[5] This annotation means that H1–H5 originate from V1, H6, and H7 from V2.

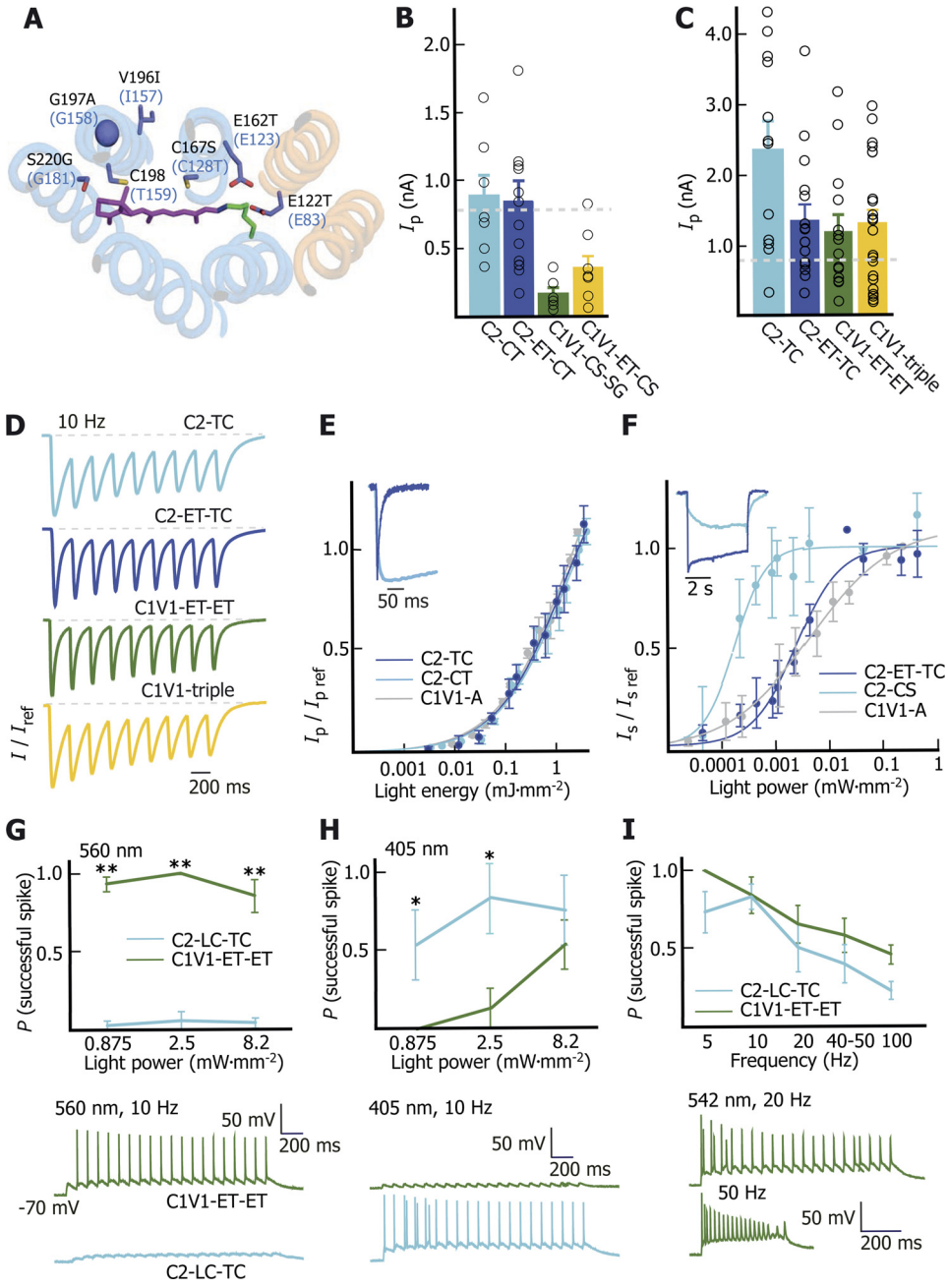

FIGURE 2. **Generation of fast- and slow-cycling color-tuned ChRs.** *A*, structural model of C1V1 based on the three-dimensional structure of C1C2–52 (Protein Data Bank code 3UG9) (23) depicting all relevant amino acid positions. *B* and *C*, average peak photocurrent amplitudes of ChRs in HEK cells at their respective peak wavelength for slow- and fast-cycling mutants (>10 mW·mm^{-2}). *D*, normalized current responses to light trains of 10 Hz for fast-cycling mutants. *E*, stimulus-response curves of peak currents I_P upon 7-ns laser flashes (n = 5, 3, and 4 for C2-TC, C2-CT and C1V1). The *inset* shows the respective current traces for C2-TC and C2-CT. *F*, light titration curve for I_S of slow- and fast-cycling mutants upon stimulation with 5-s light pulses (n = 5, 3, and 5 for C2-ET-TC, C2-CS, and C1V1). *Inset* exemplifies individual traces for C2-CS and C2-ET-TC. *G–I*, action potential firing in hippocampal neurons. *G*, at 560-nm light C1V1-ET-ET triggers spikes reliably compared with C2-LC-TC. *H*, at 405-nm light C2-LC-TC is applicative to evoke spikes at 0.875 mW·mm^{-2} whereas no spikes are seen for C1V1-ET-ET at similar intensities. By contrast, at 8.2 mW·mm^{-2} C1V1-ET-ET evokes spikes with same probability as C2-LCTC. *I*, in responding to trains of light pulses up to 20 Hz, both C2-LC-TC and C1V1-ET-ET are spiking with high fidelity. However at 40–50 Hz and above, the probability of successful spike generation is significantly reduced compared with 5 Hz (n > 4) particularly for C1V1-ET-ET.

580 nm. Moreover, this overlap of spectra also precludes optical back-conversion by a red-shifted light stimulus (supplemental Fig. 1*B*) after the actinic light is switched off. To the contrary, the red-shifted dark state is facilitating photochemical back-reaction at 400-nm light, which is more complete for C1V1-based than C2-based slow-cycling ChRs. The reason is that the photocycle intermediate Pro-390, which is in equilibrium with the conducting state (14, 15), is spectrally more separated from the dark state compared with C2-C128S.

For generation of fast-cycling C1V1 mutants we tested point mutations that had caused photocycle acceleration in other ChRs. Positions of successfully mutated residues are again shown in Fig. 2*A*. The E162T exchange (E123T in C2) resulted in 3-fold faster off-kinetics and a 20-nm blue-shifted spectrum

with some broadening of the spectrum as already published (15). The blue shift was unexpected because the corresponding ChETA mutation in C2 caused a 20-nm red shift (12). Interestingly, combining E162T with E122T (C1V1-ET-ET) prevented the spectral broadening and showed a faster $\tau_{off} \approx 15$ ms (supplemental Table 1). Because the maximal absorption of C1V1-ET-ET peaks at 528 nm, it is an alternative for C1V1-SG whenever fast repetitive green light stimulation is required. Prior to the detailed biophysical characterization we already have employed this variant of our screen for the manipulation of neocortical excitation/inhibition balance (15). To further accelerate deactivation kinetics, C1V1-ET was combined with V196I and G197A mutations in H4 (157 and 158 in C2) (Fig. 2*A*) (22), which were expected to distort the functionality of Cys-198 due to subtle structural changes. When introduced separately, the off-kinetics showed 123 and 79 ms relaxations, whereas the combination C1V1-ET-VI-GA (C1V1-triple) caused faster off-kinetics of ≈41 ms, respectively, with currents still larger than C2 currents (Fig. 2*C*). But, upon 10-Hz stimulation (Fig. 2*D*) the C1V1-triple performed with 48% inactivation and significant offset currents slightly better than C2-TC (60% inactivation) (supplemental Table 1), while underperforming relative to C2-ET-TC and C1V1-ET-ET that showed less inactivation and smaller offset currents.

To compare the real efficiency of light activation (intrinsic light sensitivity) for different ChRs in host cells, we recorded light titration curves for the early peak current I_P and the stationary current I_S for slow- and fast-cycling variants upon stimulation with 7-ns flashes and 5-s light pulses (Fig. 2, *E* and *F*). These experiments showed that the efficiency of the primary photoreaction is identical in WT C2, C1V1, and step-function ChRs, although for the last the rise time of the photocurrents is much slower (Fig. 2*E*, *inset*). In contrast, the light sensitivity of the steady-state currents I_S is a function of light absorption, lifetime of the open state, and photochemical inactivation. Consequently, step-function currents saturate at much lower steady-state light intensities (Fig. 2*F*).

We next tested wavelength-dependent spiking performance with parallel transduction of C2-LC-TC, a high conductance C2 variants discussed below, and C1V1-ET-ET in cultured hippocampal neurons (23). Spike trains were evoked by light stimulation using 3-ms pulses at frequencies of 20 Hz. Fig. 2, *G* and *H*, shows the fraction of successful spikes at the indicated wavelengths and light power densities in cells expressing C2-LC-TC or C1V1-ET-ET.

Spike elicitation at 20 Hz by 560 nm was found to confer specificity between both variants across light intensities. For 405-nm light at lower intensities it was also possible to separate activation. Irradiance values of <1 mW·mm^{-2} appeared optimal for this discrimination while still conferring good performance in C2-LC-TC-expressing neurons. We also studied the ability of both variants to reliably follow trains of light pulses delivered at a range of physiologically relevant frequencies. Despite the slower kinetics, at higher frequencies C2-LC-TC caused more reliable firing compared with C1V1-ET-ET (Fig. 2, *H* and *I*). Peak wavelengths were used to activate both groups, 470 nm for C2-LC-TC and 542 nm for C1V1-ET-ET.

For activation of two HEK cell populations with different wavelengths we compared responses of C1V1, C1V1-triple, and C2-TC at 405 or 560 nm light (Fig. 3, *A* and *B*). C1V1-triple shows full activation at 560 nm and residual activation at 405 nm that is clearly smaller than for C1V1 (*gray*). In contrast, the reaction of C2-TC is half-maximal at 405 nm with zero cross-reactivity at 560 nm. The 2-fold larger peak photocurrent of C2-TC compared with C2 provides a significant advantage for stimulation at 405 nm. Based on these results we employed a fura-2-based Ca^{2+} assay in a cell line that stably expresses a mTrek potassium channel and a voltage-gated Ca^{2+}-channel ($Ca_V3.2$) (23). At given cytoplasmic ion concentrations, the steady-state membrane voltage in darkness is controlled by extracellular potassium, and depolarization can be modulated with light via C2-TC or, alternatively, C1V1-triple. At sufficient depolarization the $Ca_V3.2$ channels open, and Ca^{2+} influx is monitored as fura-2 fluorescence as shown in the pictogram in Fig. 3*C* (24). This assay allowed us to directly compare the performance of blue- and green-absorbing ChRs for membrane depolarization. The cells displayed in Fig. 3*C* express C1V1-triple-eCFP and C2-TC-mCherry seen as cyan and red fluorescence. Excitation with 405-nm light caused a rapid decrease in fura-2 fluorescence in cells expressing C2-TC whereas 560-nm light evoked Ca^{2+} influx in the C1V1-triple-expressing cells only. Thus, the 405-nm and 560-nm light were almost perfectly selective. In contrary, 470-nm light excited both C2-TC and C1V1 equally well causing $Ca_V3.2$-mediated Ca^{2+} influx in both cell types. Light power at 405 nm of up to 0.03 mW·mm^{-2} for C2-TC excitation was used without cross-activating C1V1.

Finally, to characterize cation flux through ChRs we recorded photocurrents at various ionic conditions. We included in this survey C2-L132C (C2-LC) for which an enhanced Ca^{2+} selectivity had been reported (17). We introduced the analogous mutation into C1V1, but L171C was only weakly expressed. It was conceivable that L171C is destabilized by interaction with the Cys at position 198 (Thr-159 in C2 as shown in supplemental Fig. 3). However, the C2 double mutant C2-L132C/T159C (C2-LC-TC) showed superb performance (Fig. 3*D*). We also included in the survey both C1V1 variants, A and B. Total peak currents under standard conditions are compared in Fig. 3*D*, revealing that C1V1-B, C2-LC, C2-TC, and C2-LC-TC mediate almost 3-fold larger peak currents than WT C2, whereas C1V1-A currents were clearly smaller. Photocurrents of C2-LC-TC were most robust and consistent. Peak currents were normalized to the levels at pH_o 7.2 and 140 mM Na^+. Different grades of inactivation can be seen from individual traces in Fig. 3*E*. Next, photocurrents were measured at pH 9 and were compared with I_0 of pH_o 7.2. (Fig. 3*F*). At 2 mM Ca^{2+} and 2 mM Mg^{2+} conductances were small as expected, but the I_S was significantly larger for C2-LC and C2-LC-TC. At 140 mM Na^+ the I_0 was only slightly enlarged for C1V1, C2-LC, C2-TC, and C2-LC-TC compared with WT C2. But, this increase was even more obvious at high Ca^{2+}, suggesting that all four variants have particularly enhanced Ca^{2+}-selectivity (Fig. 3*F*, *upper panel*, and supplemental Fig. 2*A*). Notably, for Ca^{2+}-influx in continuous light the stationary current I_S is of much higher relevance than the peak currents I_0. Our experiments show that I_S under high Ca^{2+} is large for C1V1, C2-LC, and C2-LC-TC,

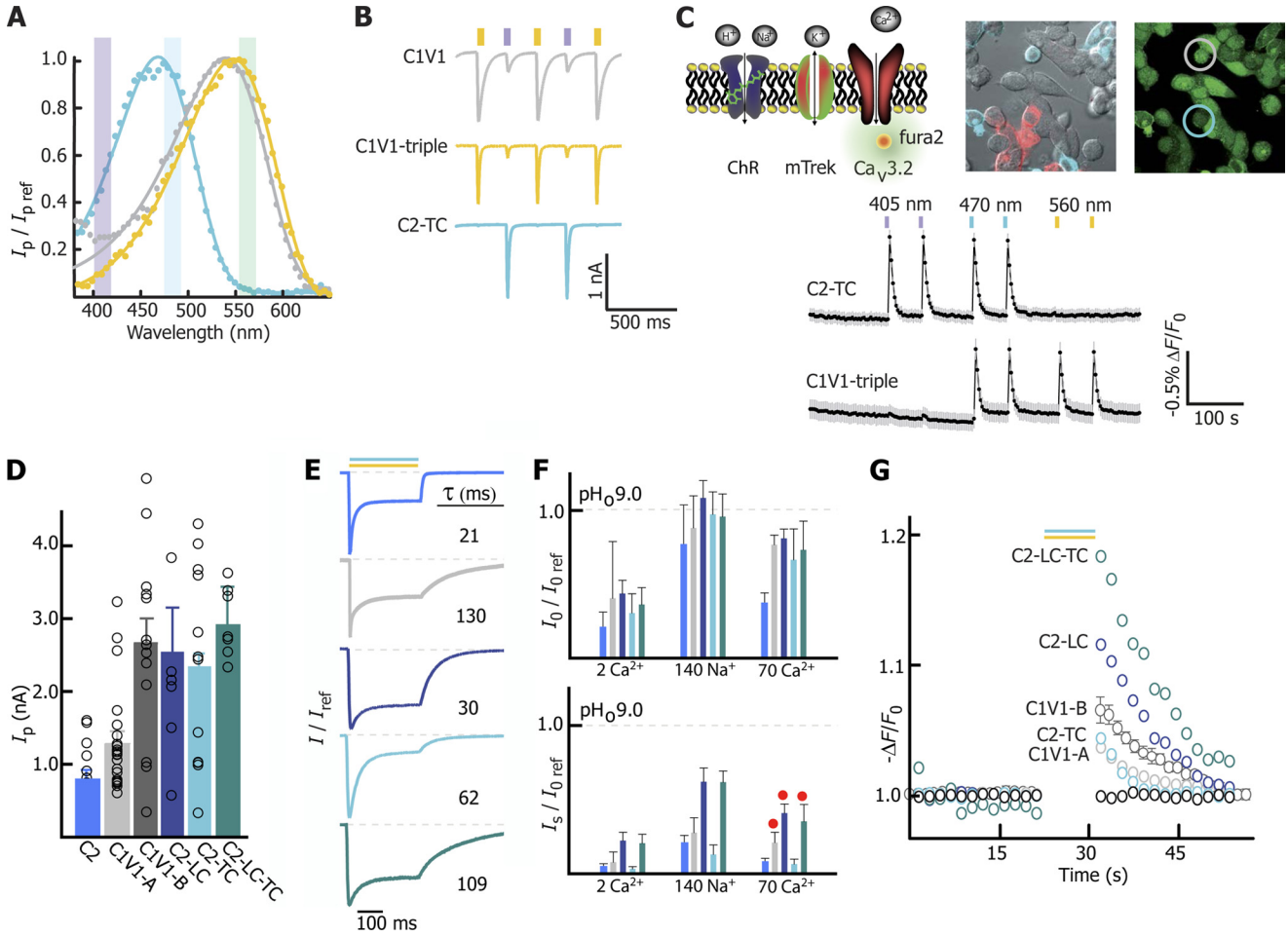

FIGURE 3. **Dual light excitation and ion selectivity for blue and green light-absorbing ChRs.** *A*, action spectra for C2-TC (*blue*), C1V1 (*gray*), and C1V1-triple (*orange*) ($n = 2$, 8, and 9). Excitation at 405, 470, and 560 nm is indicated by *colored bars*. *B*, responses of C2-TC, C1V1, and C1V1-triple upon 10-ms light pulses at 405 and 560 nm. *C*, Ca^{2+} response in two mixed cell populations. Membrane potential was adjusted through mTrek potassium channel with extracellular K^+. Ca^{2+} influx through $Ca_V3.2$ was monitored by a change in fura-2 fluorescence. HEK cells were separately transfected with C1V1-triple-eCFP and C2-TC-mCherry are shown as fluorescence and transmission overlay (*left*) and as fura-2 emission (*right*). Corresponding fura-2 traces for *cyan* and *red* fluorescent cells are shown underneath (two trials with 8 and 13 cells for C2-TC and C1V1-triple). *D* and *E*, peak photocurrent amplitudes and profiles for C2, C1V1-A, C1V1-B (both exhibit virtually identical profiles), C2-LC, C2-TC, and C2-LC-TC for 300-ms light pulses. *F*, average initial currents (*upper panel*) and stationary photocurrents with S.D. (*lower panel*) at different ionic conditions. Intracellular buffer was kept at 110 mM *N*-methyl-D-glucamine-Tris, pH_i 9.0. Currents were normalized to I_0 at standard conditions. All data points are evaluated at −60 mV (each $n > 8$). *G*, fura-2 fluorescence in ChR-expressing HEK cells after light stimulation for 10 s (*black bar*) at an extracellular $CaCl_2$ concentration of 70 mM at pH_o 7.2 ($n > 10$ cells). Fluorescence intensity before light application is normalized to 1.

but is small for C2-TC and WT C2 (Fig. 3*F*, *lower panel*, and supplemental Fig. 2*B*, *red traces*). In summary, at −60 mV and symmetric pH 9, C2-LC-TC shows 7.4-fold larger Ca^{2+} peak currents (I_P) and 19 times larger I_S compared with C2 (Fig. 3, *D–F*) taking the normalization into account (supplemental Table 2). C1V1-B shows 7.1-fold larger I_0 and 10-fold larger I_S under similar conditions. However, this enhancement might be quite different at higher voltage (less negative) and low pH. Because Ca^{2+}-mediated currents are superimposed by proton currents at neutral pH_o, the Ca^{2+} fraction of the inward current is difficult to distill from electrical recordings at neutral pH_o (Fig. 4, *D* and *E*). Thus, we visualized the Ca^{2+} influx again by a fura-2-based Ca^{2+} assay (Fig. 3*G*). Whereas C1V1-A showed only slightly higher Ca^{2+} influx because of its only moderately improved expression, C1V1-B delivered significantly higher Ca^{2+} influx than C2-TC and C1V1-A due to its higher expression level. However, the fura-2 assay also revealed that C2-LC and particularly C2-LC-TC under neutral conditions promote higher Ca^{2+} influx in continuous light, under conditions of competition with H^+.

DISCUSSION

We applied a helix exchange strategy to *Volvox* V1 and revealed a well expressing C1V1 chimera with a 70-nm red-shifted absorption relative to the commonly used C2. We also showed that the earlier reported kinetic tuning of C2 can be transferred to the new C1V1 chimera, although the effects of individual mutations differ quantitatively and substantially from related mutations in C2. By a systematic exchange of V1 helices by V2 homologs we identified the helices H6 and H7 as the most essential for the absorption difference between V1 (535 nm) and V2 (465 nm), and helices H1 and H2 as most critical for good expression. Certainly, it was conceivable that the 39 extra amino acids in the N-terminal region of C1 contain sequences or even single amino acids that are responsible for better membrane integration or folding, although both of the

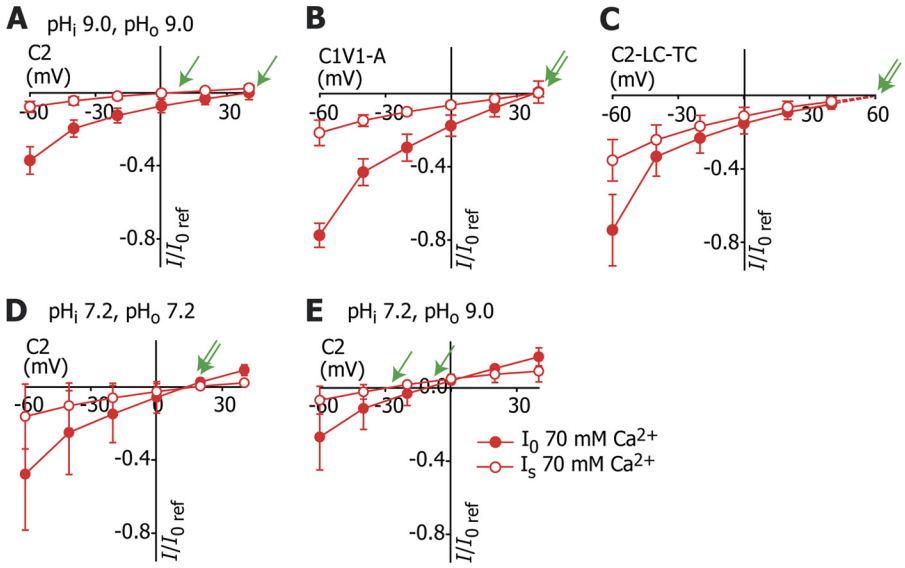

FIGURE 4. **Current-voltage relationships for C2, C1V1-A, and C2-LC-TC.** Photocurrents were recorded at high Ca^{2+} (70 mM) and variable internal pH ($pH_i = 9$ for *A–C*, $pH_i = 7.2$ for *D* and *E*). Reversal potentials of initial currents I_0 (*filled circles*) and stationary currents I_S (*open circles*) are indicated by *green arrows* ($n > 8$).

parental V1 and C1 rhodopsins are poorly expressed. Therefore, we suggest that interaction between helix H1 and H7 is the most relevant parameter for the excellent membrane integration of C1V1, also in accordance with the C1C2 structure (22). A light-dependent modulation of the tilting angle between H1 and H7 could be a molecular mechanism for opening and closing of the ion channel pore formed by H1, H2, H6, and H7 (22). To test this hypothesis an open state crystal structure is mandatory. Nevertheless, even small differences in the EC-L1 loop region, as between C1V1-A and B, can have variable effects on the expression level in different host systems. Moreover, the natural presence of Cys at position 198 (Thr-159 in C2) is an additional factor for effective membrane integration as shown by the large C2-TC currents and the small currents of the C1V1-C198T. As noted above, the mutation E122T in C1V1 (Glu-83 in C2) showed an extra 5-nm bathochromic shift to 545 nm rendering it the most red-shifted ChR so far. Rather unexpected was the blue shift of E162T, a mutation that caused a red shift in C2 (E123T in C2) (12). Thus, the arrangement of counterion of the protonated retinal Schiff base must be different in C1V1 compared with C2, probably allowing anions such as Cl^- to replace the Glu in the case of C1V1-ET but not in C2-ET. Any approach to shift the C1V1-ET absorption further in the bathochromic directions by single mutations was unsuccessful; further color tuning will therefore likely rely on several subtle amino acids exchanges, which then synergistically shift absorption. This remains a difficult task even with a high resolution structure in hand because the counterion arrangement remains difficult to modify. A promising alternative is complementary mining of genomic databases of other algae or other lower eukaryotes for natural red-shifted ChRs that can in turn be further modified according to the strategy outlined here. Because modification of Asp-195 in C1V1 did not result in a slower photocycle (in contrast to similar changes of the homologous residue Asp-156 in C2), we can effectively rule out the direct interaction of Asp-195 with Cys-167 (Asp-156 to Cys-128 in C2) as proposed by Bamann *et al.* for C2 (14) (see supplemental Fig. 3*A*). It is also intriguing that C2-based slow ChRs can be switched off with 405- and 590-nm light, whereas C1V1-based versions are only efficiently inactivated by 405 nm. As we proposed above, this observation can be elegantly explained by a close overlap of the dark-state spectrum with the spectrum of the conducting state due to a smaller absorption shift of the latter. This would also explain, at least partially, why the maximal currents of the C1V1-based step-function tools are small.

In Fig. 3 we show that the early Ca^{2+} current I_0 of C1V1 is larger than I_0 of C2 and about equal to I_0 of C2-LC at pH_o 9, whereas the stationary C1V1 Ca^{2+} current is 2-fold smaller compared with C2-LC or C2-LC-TC. However, Ca^{2+} competes with other ions as we recently evaluated quantitatively for WT C2 and some mutants (16). This competition is quite different for I_0 and I_S as seen from the *I-V* plots in Fig. 4 and supplemental Fig. 2. For C2 the reversal potential E_r, for I_0 at 70 mM Ca^{2+} pH_o 9 and pH_i 9 is near +45 mV and is near zero at 2 mM Ca^{2+}. This shift correlates with the Nernst potential change and suggests that at 70 mM Ca^{2+} most of the current is carried by Ca^{2+} and very little Ca^{2+} is conducted at 2 mM Ca^{2+} (supplemental Fig. 2*A*). To the contrary, for the stationary current I_S E_r is still zero at 70 mM Ca^{2+} (Fig. 4*A*), indicating that the contribution of Ca^{2+} to I_S is very minor even at high Ca^{2+}. It was puzzling to see that at neutral $pH_{o/i}$ the differences in the reversal potentials disappear (Fig. 4*D*), whereas at neutral internal pH_i and high external pH_o H^+ efflux is dominating photocurrents but with a higher influence on I_S compared with I_0 (E_r for I_S is more negative than E_r for I_0 (Fig. 4*E*). This again supports the idea that internal and external protons compete with Ca^{2+} especially during the stationary phase. For C1V1 the situation is qualitatively and quantitatively different. At $pH_{o/i} = 9$ E_r for both I_0 and I_S is similar to the E_r for I_0 of C^2, suggesting that in C1V1, the channel selectivity has not changed during adaptation. Similarly, in C2-LC-TC, both E_r for I_0 and I_S are again very similar but more positive, indicating that C2-LC-TC is even more

Ca^{2+}-selective than C1V1. The greater Ca^{2+} influx of C2-LC-TC (and with some reduction of C1V1) as seen in the fura-2 assays is multifactorial, and the 2-fold higher Ca^{2+} selectivity is only one contributory factor. Equally important is the 3-fold better expression, lower inactivation, and reduced H^+ competition. Consistent with these HEK cell measurements, our neuronal experiments revealed an improved performance for C2-LC-TC (CatCh+) and C1V1. Both variants provide the cells an improved operational light sensitivity (Fig. 2*G*) and therefore allowed a better dual-color activation at lower light intensities compared with previous studies with wild type V1 (20). Surprisingly, C2-LC-TC enabled successful spiking similar to C2 despite its 10 times slower off-kinetics (14) (Fig. 2*I*), supporting the assumption that higher Ca^{2+} permeability may facilitate faster repolarization through activation of secondary channels (17). Because the LC mutation results in nonfunctional C1V1, we conclude that the best Ca^{2+}-conducting variant for green and yellow light stimulation remains C1V1-B.

Acknowledgments—We thank Maila Reh and Petra Klein for excellent technical assistance, Dietrich Gradmann for intense and fruitful discussion, Andreas Herrmann and Thomas Korte for help with confocal microscopy, and Ofer Yizhar for constructing the C1V1-B variant and proofreading the manuscript.

REFERENCES

1. Nagel, G., Ollig, D., Fuhrmann, M., Kateriya, S., Musti, A. M., Bamberg, E., and Hegemann, P. (2002) Channelrhodopsin-1: a light-gated proton channel in green algae. *Science* **296,** 2395–2398
2. Nagel, G., Szellas, T., Huhn, W., Kateriya, S., Adeishvili, N., Berthold, P., Ollig, D., Hegemann, P., and Bamberg, E. (2003) Channelrhodopsin-2, a directly light-gated cation-selective membrane channel. *Proc. Natl. Acad. Sci. U.S.A.* **100,** 13940–13945
3. Zhang, F., Wang, L. P., Boyden, E. S., and Deisseroth, K. (2006) Channelrhodopsin-2 and optical control of excitable cells. *Nat. Methods* **3,** 785–792
4. Douglass, A. D., Kraves, S., Deisseroth, K., Schier, A. F., and Engert, F. (2008) Escape behavior elicited by single, channelrhodopsin-2-evoked spikes in zebrafish somatosensory neurons. *Curr. Biol.* **18,** 1133–1137
5. Han, X., Qian, X., Bernstein, J. G., Zhou, H. H., Franzesi, G. T., Stern, P., Bronson, R. T., Graybiel, A. M., Desimone, R., and Boyden, E. S. (2009) Millisecond-timescale optical control of neural dynamics in the nonhuman primate brain. *Neuron* **62,** 191–198
6. Bi, A., Cui, J., Ma, Y. P., Olshevskaya, E., Pu, M., Dizhoor, A. M., and Pan, Z. H. (2006) Ectopic expression of a microbial-type rhodopsin restores visual responses in mice with photoreceptor degeneration. *Neuron* **50,** 23–33
7. Kravitz, A. V., Freeze, B. S., Parker, P. R., Kay, K., Thwin, M. T., Deisseroth K., and Kreitzer, A. C. (2010) Regulation of parkinsonian motor behaviours by optogenetic control of basal ganglia circuitry. *Nature* **466,** 622–626
8. Bruegmann, T., Malan, D., Hesse, M., Beiert, T., Fuegemann, C. J., Fleischmann, B. K., and Sasse, P. (2010) Optogenetic control of heart muscle *in vitro* and *in vivo*. *Nat. Methods* **7,** 897–900
9. Llewellyn, M. E., Thompson, K. R., Deisseroth, K., and Delp, S. L. (2010) Orderly recruitment of motor units under optical control *in vivo*. *Nat. Med.* **16,** 1161–1165
10. Johansen, J. P., Hamanaka, H., Monfils, M. H., Behnia, R., Deisseroth, K., Blair, H. T., and LeDoux, J. E. (2010) Optical activation of lateral amygdala pyramidal cells instructs associative fear learning. *Proc. Natl. Acad. Sci. U.S.A.* **107,** 12692–12697
11. Berndt, A., Prigge, M., Gradmann, D., and Hegemann, P. (2010) Two open states with progressive proton selectivities in the branched channelrhodopsin-2 photocycle. *Biophys. J.* **98,** 753–761
12. Gunaydin, L. A., Yizhar, O., Berndt, A., Sohal, V. S., Deisseroth, K., and Hegemann, P. (2010) Ultrafast optogenetic control. *Nat. Neurosci.* **13,** 387–392
13. Berndt, A., Yizhar, O., Gunaydin, L. A., Hegemann, P., and Deisseroth, K. (2009) Bi-stable neural state switches. *Nat. Neurosci.* **12,** 229–234
14. Bamann, C., Gueta, R., Kleinlogel, S., Nagel, G., and Bamberg, E. (2010) Structural guidance of the photocycle of channelrhodopsin-2 by an interhelical hydrogen bond. *Biochemistry* **49,** 267–278
15. Yizhar, O., Fenno, L. E., Prigge, M., Schneider, F., Davidson, T. J., O'Shea, D. J., Sohal, V. S., Goshen, I., Finkelstein, J., Paz, J. T., Stehfest, K., Fudim, R., Ramakrishnan, C., Huguenard, J. R., Hegemann, P., and Deisseroth, K. (2011) Neocortical excitation/inhibition balance in information processing and social dysfunction. *Nature* **477,** 171–178
16. Gradmann, D., Berndt, A., Schneider, F., and Hegemann, P. (2011) Rectification of the channelrhodopsin early conductance. *Biophys. J.* **101,** 1057–1068
17. Kleinlogel, S., Feldbauer, K., Dempski, R. E., Fotis, H., Wood, P. G., Bamann, C., and Bamberg, E. (2011) Ultra light-sensitive and fast neuronal activation with the Ca^{2+}-permeable channelrhodopsin CatCh. *Nat. Neurosci.* **14,** 513–518
18. Wang, H., Sugiyama, Y., Hikima, T., Sugano, E., Tomita, H., Takahashi, T., Ishizuka, T., and Yawo, H. (2009) Molecular determinants differentiating photocurrent properties of two channelrhodopsins from *Chlamydomonas*. *J. Biol. Chem.* **284,** 5685–5696
19. Zhang, F., Prigge, M., Beyrière, F., Tsunoda, S. P., Mattis, J., Yizhar, O., Hegemann, P., and Deisseroth, K. (2008) Red-shifted optogenetic excitation: a tool for fast neural control derived from *Volvox carteri*. *Nat. Neurosci.* **11,** 631–633
20. Kianianmomeni, A., Stehfest, K., Nematollahi, G., Hegemann, P., and Hallmann, A. (2009) Channelrhodopsins of *Volvox carteri* are photochromic proteins that are specifically expressed in somatic cells under control of light, temperature, and the sex inducer. *Plant Physiol.* **151,** 347–366
21. Zhang, F., Wang, L. P., Brauner, M., Liewald, J. F., Kay, K., Watzke, N., Wood, P. G., Bamberg, E., Nagel, G., Gottschalk, A., and Deisseroth, K. (2007) Multimodal fast optical interrogation of neural circuitry. *Nature* **446,** 633–639
22. Kato, H. E., Zhang, F., Yizhar, O., Ramakrishnan, C., Nishizawa, T., Hirata, K., Ito, J., Aita, Y., Tsukazaki, T., Hayashi, S., Hegemann, P., Maturana, A. D., Ishitani, R., Deisseroth, K., and Nureki, O. (2012) Crystal structure of the channelrhodopsin light-gated cation channel. *Nature*, **482,** 369–374
23. Berndt, A., Schoenenberger, P., Mattis, J., Tye, K. M., Deisseroth, K., Hegemann, P., and Oertner, T. G. (2011) High-efficiency channelrhodopsins for fast neuronal stimulation at low light levels. *Proc. Natl. Acad. Sci. U.S.A.* **108,** 7595–7600
24. Prigge, M., Rösler, A., and Hegemann, P. (2010) Fast, repetitive light-activation of $Ca_V3.2$ using channelrhodopsin 2. *Channels* **4,** 241–247
25. Tian, L., Hires, S. A., Mao, T., Huber, D., Chiappe, M. E., Chalasani, S. H., Petreanu, L., Akerboom, J., McKinney, S. A., Schreiter, E. R., Bargmann, C. I., Jayaraman, V., Svoboda, K., and Looger, L. L. (2009) Imaging neural activity in worms, flies and mice with improved GCaMP calcium indicators. *Nat. Methods* **6,** 875–881